CASL-X-2016-1104-000

Power uprates
and plant life extension

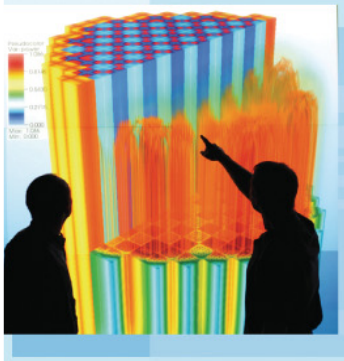

Engineering design
and analysis

Science-enabling
high performance
computing

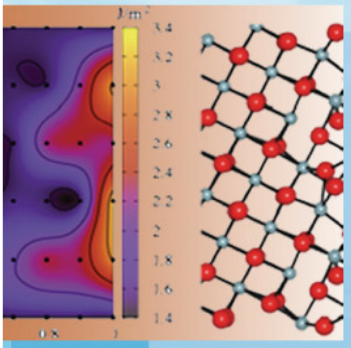

Fundamental science

Plant operational data

Consortium for Advanced Simulation of LWRs

Reactivity Insertion Accident (RIA) Capability Status in the BISON Fuel Performance Code

U.S. DEPARTMENT OF ENERGY | Nuclear Energy

Oak Ridge National Laboratory

in partnership with

Electric Power Research Institute
Idaho National Laboratory
Los Alamos National Laboratory
Massachusetts Institute of Technology
North Carolina State University
Sandia National Laboratories
Tennessee Valley Authority
University of Michigan
Westinghouse Electric Company

REVISION LOG

Revision	Date	Affected Pages	Revision Description
0	05/30/2016	All	Original version

Reactivity Insertion Accident (RIA) Capability Status in the BISON Fuel Performance Code

R. L. Williamson, C. P. Folsom, G. Pastore, S. Veeraraghavan
Fuels Modeling & Simulation Department
Idaho National Laboratory
Idaho Falls, ID

May 25, 2016

Contents

Acronyms

CRDA	Control Rod Drop Accident
CSNI	Committee on Safety of Nuclear Installations
CZP	Cold Zero Power
DNB	Departure from Nucleate Boiling
FCT	Fuel Centerline Temperature
FGR	Fission Gas Release
FWHM	Full Width at Half Maximum
HZP	Hot Zero Power
INL	Idaho National Laboratory
JFNK	Jacobian Free Newton Krylov
LWR	Light Water Reactor
LOCA	Loss of Coolant Accident
MOOSE	Multiphysics Object Oriented Simulation Environment
NEA	Nuclear Energy Agency
OECD	Organization for Economic Co-operation and Development
REA	Rod Ejection Accident
RIA	Reactivity Insertion Accident
USNRC	US Nuclear Regulatory Commission
WGFS	Working Group on Fuel Safety
V&V	Verification and Validation

1 Introduction

As summarized in the CASL Reactivity Insertion Accident (RIA) Challenge Problem Charter [1]: "The PWR REA and BWR CRDA are postulated accidents with consequences that are important to nuclear safety (fuel rod integrity and core coolability). Currently each reload core design must be analyzed to meet regulatory acceptance criteria. The goal of CASLs ModSim capability for RIA is to model the event at a higher fidelity, with validation to existing tests, to better model the transient neutronics and the progression of the fuel and cladding thermal-mechanical behavior. These improved analytical capabilities can be used to better inform reload core design, limits on fuel assembly discharge burnup, restrictions on placement of fuel in the reactor, control rod insertion limits, operating margin, and performance sensitivities."

In accordance with that charter, a CASL RIA Challenge Problem has been defined as described in [2]. BISON is the fuel performance code used within CASL for LWR fuel under both normal operating and accident conditions, and thus must be capable of addressing the RIA challenge problem. The purpose of this report is to outline required BISON capabilities for RIAs and describe the current status of the code. Information on recent accident capability enhancements, application of BISON to a RIA benchmark exercise, and plans for validation to RIA behavior are included.

This report begins with a brief background description of BISON including identification of code dependencies. Capability requirements and current status for RIA simulation are then described, including a chapter on recent capability enhancements specific to accident analysis. A chapter is included describing application of BISON to the current Organization for Economic Co-operation and Development (OECD) RIA benchmark exercise, including comparisons to another accident analysis code. A final chapter describes verification and validation activities for BISON and identifies specific RIA validation cases planned for the future.

2 BISON Description

2.1 Tool Description

BISON is a modern finite-element based nuclear fuel performance code that has been under development at the Idaho National Laboratory (USA) since 2009 [3]. The code is applicable to both steady and transient fuel behavior and can be used to analyze 1D (spherically symmetric), 2D (axisymmetric and generalized plane strain) or 3D geometries. BISON has been used to investigate a variety of fuel forms including LWR oxide fuel [3], TRISO coated-particle fuel [4] and metallic fuel in rod and plate form [5, 6]. The code has also been used to design and to interpret irradiation experiments [7] and investigate novel fuel concepts [8].

BISON is built using the INL Multiphysics Object-Oriented Simulation Environment, or MOOSE [9]. MOOSE is a massively parallel, finite element-based framework to solve systems of coupled non-linear partial differential equations using the Jacobian-Free Newton Krylov (JFNK) method [10]. This enables investigation of computationally large problems, for example a full stack of discrete pellets in a LWR fuel rod, or every rod in a full reactor core. MOOSE supports the use of complex two and three-dimensional meshes and uses implicit time integration, important for the widely varied time scale in nuclear fuel simulation. An object-oriented architecture is employed which greatly minimizes the programming effort required to add new material and behavioral models.

The BISON governing relations currently consist of fully-coupled partial differential equations for energy, species, and momentum conservation. Users can select a subset of these equations (e.g., energy and momentum for thermomechanics analysis) within the input file. The code employs both nonlinear kinematics, which accounts for large deformation, and nonlinear material behavior. A detailed description of the nonlinear kinematics is provided in [3]. For nonlinear plasticity and creep, strains are calculated implicitly utilizing the radial return method; the specific procedure is outlined in [11].

Focusing initially on UO_2 fuel, models are included in BISON to describe temperature and burnup dependent thermal properties, solid and gaseous fission product swelling, densification, thermal and irradiation creep, fracture via relocation or smeared cracking, and fission gas production, generation, and release.

Recently an improved fission gas release model was implemented in BISON, based on the work of Pastore et al. [12]. While retaining a physics-based description of the relevant mechanisms, the model is characterized by a level of complexity suitable for application to engineering-scale nuclear fuel analysis and consistent with the uncertainties pertaining to key input parameters. The treatment includes the fundamental features of fission gas behavior, among which are gas diffusion and precipitation in fuel grains, growth and coalescence of gas bubbles at grain faces, grain growth and grain boundary sweeping effects, thermal, athermal, and transient gas release.

Focusing initially on Zircaloy as a cladding material, models are available for instantaneous plasticity, thermal and irradiation creep, and irradiation growth. The plasticity and creep models can be applied simultaneously, in cases where both phenomena are active.

Gap heat transfer is modeled in the traditional manner with the total conductance across the gap computed as a sum of the gas conductance, the increased conductance due to solid-solid contact, and the conductance due to radiant heat transfer [13]. This model is typically applied between the fuel and cladding, but can also be used to simulate heat transfer between individual pellets, between a pellet and end cap, or between fracture surfaces.

Mechanical contact between materials is implemented through the use of node/face constraints, which prevent nodes on one side of an interface from penetrating faces on the other side of the interface [14].

For LWR fuel, the pressure in the gap and plenum is computed assuming a single cavity volume and using the ideal gas law. The moles of gas, the temperature, and the cavity volume are free to change with time. The moles of gas at any time are computed as the original amount of gas (computed based on original pressure, temperature, and volume) plus the amount in the cavity due to fission gas released. The gas temperature is computed as a weighted average of the pellet exterior and cladding interior surfaces, with weighting based on an approximation of the volume of gas contained between the solid surfaces. The cavity volume is computed as needed based on the evolving pellet and cladding geometry.

2.2 Code dependencies: Software and Hardware

BISON depends on several underlying software libraries. These libraries provide the finite element framework, solver technology, parallel communication, and various other functionalities. A summary of these packages is given in Table 2.1.

Table 2.1: Software libraries used by BISON.

Library	Origin	Purpose
MOOSE[9]	Idaho National Laboratory	Finite element framework, integrates other packages for application use
libMesh[15]	The University of Texas at Austin	Parallel, unstructured mesh, numerical simulation platform
PETSc[16]	Argonne National Laboratory	Parallel linear and nonlinear equation solvers
hypre[17]	Lawrence Livermore National Laboratory	Parallel preconditioners
MPI (Open-MPI, e.g.)	Open source consortium	Message passing on parallel computers

To make the use of these libraries consistent, the MOOSE team provides installation packages

for multiple computer architectures. The packages supply pre-compiled libraries and a simple installation procedure. It is also possible to install the libraries individually if necessary.

BISON has been tested on several architectures. The bulk of the development work occurs on Apple workstations and laptops. The code is also tested on Linux machines with a variety of compilers. BISON runs on a single CPU on a laptop computer and on hundreds of CPUs on large parallel machines.

3 Capability Requirements and Status

BISON has been identified as a key computational tool for the CASL RIA Challenge Problem. An implementation plan for this challenge problem has recently been developed [2], which outlines required BISON capabilities. The following sections identify these required capabilities, provide current status including references to applicable documentation, and outline development plans where needed.

3.1 Multidimensional Heat Transfer and Solid Mechanics

The BISON governing relations consist of fully-coupled partial differential equations for energy, species, and momentum conservation [3, 18]. Users can select a subset of these equations (e.g., energy and momentum for thermomechanics analysis) within the input file. For LWR fuel, the code can be used in either 2D (axisymmetric or generalized plane-strain) or 3D. Capability is available to couple a full rod 2D axisymmetric analysis to a 2D slice or 3D submodel.

3.2 Transient Modeling Capability

The energy and species conservation equations in BISON include transient behavior [3]. The code uses implicit time integration, important for the widely varied time scales in nuclear fuel simulation. BISON also includes a variety of time step control algorithms which can be used to control time stepping based on solution error, convergence difficulty or other parameters [19]. Recently added to the code is the ability to control time stepping based on strain rate. This capability, described in greater detail in Section 4.3 was added specifically for use in accident analyses such as RIAs.

3.3 Axial and Radial Power Profiles

The thermal power in fuel rod materials can be prescribed either by coupling to an external neutronics calculation or via a user provided rod-average linear heat generation rate. The rod average power can then be partitioned within the rod using both axial and radial power profiles. The axial profile must be specified by the user. The radial profile is computed using the TUBRNP model of Lassmann [20], as described in greater detail in [18].

3.4 Pellet-Cladding Interaction

3.4.1 Gap Heat Transfer

Gap heat transfer is modeled in the traditional manner with the total conductance across the gap computed as a sum of the gas conductance, the increased conductance due to solid-solid contact, and the conductance due to radiant heat transfer [13]. Jump distances are determined using the Kennard model [21]. The thermal conductivity of the gap gas is altered based on fission gas or helium released from the fuel. This capability is described in detail in [3, 18].

3.4.2 Mechanical Contact

Mechanical contact model is computed based on the methodology of Heinstein and Laursen [22], which utilizes node to face constraints to prevent nodes on one surface from penetrating the face of another surface. The evolution of the gap width is determined using a geometric search algorithm. This capability is described in detail in [18].

3.5 Fuel Material Behavior

3.5.1 Thermal and Mechanical Properties

A variety of empirical correlations are available to describe the temperature and irradiation dependent thermal conductivity of UO_2. Examples include: 1) the Fink-Lucuta approach which employs the Fink correlation for the temperature dependence of unirradiated material [23] and a series of corrections given by Lucuta to account for the effects of porosity and irradiation [24] and 2) the NFIR correlation developed from thermal diffusivity measurements on specimens irradiated up to burnup levels of 80 MWd/kgU [25]. All available correlations are described in [18]. The ability to provide a user-defined thermal conductivity function is also available.

Accurate prescription of the fuel specific heat is critical for RIA applications. The temperature dependent specific heat of UO_2 can be specified using available empirical models [18] or provided by a user-defined function.

Elastic mechanical properties including Young's modulus, Poisson's ratio and the coefficient of thermal expansion can each be specified in two ways. The values can be given directly, or can be computed using MATPRO correlations [18].

3.5.2 Pellet Cracking and Relocation

In UO_2 fuel, a large temperature gradient develops from the fuel center to the radial edge. This gradient appears early and is strong enough to induce cracking in the fuel due to the associated stresses. Modeling fracture is important since cracks significantly reduce the stress state in the fuel and increase the effective fuel volume (i.e., decrease the fuel-cladding gap width). Two approaches are available in BISON to account for pellet fracture: relocation and smeared cracking. Relocation models are highly empirical and simply impose radial strains in the fuel to reduce the gap width, generally as a function of power and burnup. Smeared cracking models follow the approach originally outlined in [26], where cracking is simulated by adjusting the elastic

constants at material points. This is in contrast to a discrete cracking model, where topographic changes are made to the computational mesh. Note that discrete fracture models have recently been applied to oxide fuel [27, 28], but are not yet in common use in BISON.

3.5.3 Fission Gas Release

Fission gas release (FGR) is computed by a physics-based model that draws on the approach described in [12]. While retaining a level of complexity suitable for application to engineering scale fuel analysis and consistent with the uncertainties pertaining to some parameters, the model incorporates a direct description of the fundamental physical processes of gas generation, diffusion and precipitation in grains, growth and coalescence of gas bubbles at grain faces, and thermal gas release. Fission gas release and gaseous swelling are modeled as inherently coupled. This model also captures the rapid fission gas release kinetics (burst release) during transients [29]. The applicability of this burst release model to rapid RIA transients has not been demonstrated and will be the subject of further investigation.

3.6 Cladding Material Behavior

3.6.1 Thermal and Mechanical Properties

The thermal properties of Zircaloy cladding can be input directly or provided as a function of temperature based on user-defined functions. Elastic mechanical properties including Young's modulus, Poisson's ratio and the coefficient of thermal expansion can given directly or computed using MATPRO correlations [19].

3.6.2 Thermal and Irradiation Creep

During irradiation, Zircaloy cladding initially creeps inward due to the large pressure differential imposed by the reactor coolant. Once fuel-cladding gap closure occurs, the clad reverses direction and creeps outward in response to fuel swelling. Both thermal and irradiation creep mechanisms are active at typical operating conditions and are generally modeled using empirical relationships. In BISON, the Limbäck model [30] is used for primary and secondary thermal creep and provides the creep strain rate as a function of temperature, stress and time. Irradiation induced creep is modeled using the Hoppe correlation [31] which relates the creep strain rate to stress and fast neutron flux. Both are described in detail in [18]. Creep models are not expected to be active during the short time frame of a RIA, but are important in establishing the fuel rod state prior to an accident.

3.6.3 Irradiation Growth

Zircaloy undergoes irradiation-induced changes in dimensions in the absence of applied stress. In cladding this dimensional growth is principally in the axial direction and is referred to as irradiation growth. Empirical models are generally used to describe this behavior and simply describe the axial growth strain as a function of the fast neutron fluence. BISON employs the

ESCORE model described in [32, 18]. Irradiation growth is not expected to be active during the short time frame of a RIA, but is important in establishing the fuel rod state prior to an accident.

3.6.4 Oxidation

Zircaloy cladding reacts with coolant water to form an oxide layer on the cladding outer diameter. This oxide film can affect both the thermal and mechanical properties of the cladding. At normal operating temperature the oxide layer growth is calculated in two stages: a pre-transition process that follows a cubic time dependence up to a transition oxide thickness, and a post-transition process that follows a linear time dependence. BISON employs the model described in [33], where rate constants are defined in terms of coolant and cladding chemistry and fast neutron flux. At higher cladding temperatures (e.g., accident conditions) when the coolant begins to vaporize, oxidation proceeds at a much more rapid rate and is described by a parabolic law with the reaction rate constant defined as a function of temperature through an Arrhenius relation [18].

3.6.5 Hydride Formation

Concurrent with the oxidation process, hydrogen is absorbed into the cladding and diffuses under the influences of both temperature and stress. Due to the low solubility of hydrogen in Zircaloy, hydrogen can precipitate as hydrides which are brittle and known to reduce the ductility of the cladding material. BISON models for hydrogen diffusion in Zircaloy under both mass and temperature gradients, including precipitation and dissolution of hydrides, are reported in [18, 34]. The impact of hydrides on cladding mechanical behavior and potential failure is not currently addressed in BISON and is a topic of future work.

3.6.6 Plasticity, Ballooning and Rupture

A Zircaloy plasticity model applicable at high temperatures and strain-rates was recently implemented in BISON and is described in detail in Section 4.1. This model has been successfully used to simulate the OECD RIA benchmark cases, as descried in Chapter 5.

As described in [18], the mechanics formulation in BISON is based on nonlinear kinematics, thus the code is applicable to large deformations, such as clad ballooning during accidents.

Another recent addition to BISON is a Zircaloy cladding burst model, as described in Section 4.2. This model has been calibrated using burst data for power ramp rates much slower than those expected in a RIA and thus must be validated against RIA experiments before being used with confidence. Note that the current burst model does not include explicit cracking, rather it provides a prediction of when cracking will occur based on local stress and strain conditions in the cladding.

3.7 Effects of CRUD

BISON currently has no capability to include the effects of a CRUD layer. A first step will be to assess the importance of CRUD to RIA analysis.

3.8 Coolant Behavior

BISON currently includes a simplified coolant channel model that computes coolant temperature rise in a 1-D coolant channel based on calculation of the mode of heat transfer and a variety of convective heat transfer correlations [18]. The model is principally applicable to steady reactor operations and not intended for application to rapid transient behavior, such as in a RIA. BISON can be readily coupled to thermal hydraulics codes such as CTF and RELAP7 for application to such behavior.

4 Recent Capability Enhancements

4.1 Cladding Plasticity

A Zircaloy plasticity model applicable to high temperatures and strain rates was recently implemented from [35]. Before yield, the stress-strain relationship follows Hooke's law, i.e.,

$$\sigma = E\varepsilon \tag{4.1}$$

where σ is the stress, ε is the total strain and E is the Young's modulus.

After yield, the stress-strain relationship follows a power law as shown below

$$\sigma = K\varepsilon^n \left(\frac{\dot{\varepsilon}}{10^{-3}} \right)^m \tag{4.2}$$

where K is the strength coefficient, n is the strain hardening exponent, m is the strain rate exponent and $\dot{\varepsilon}$ is the strain rate. Note that the total strain (ε) is used in the above expression.

The yield stress (σ_y) is then the non-zero intersection of the above two equations and is given by

$$\sigma_y = \left[\frac{K}{E^n} \left(\frac{\dot{\varepsilon}}{10^{-3}} \right) \right]^{\left(\frac{1}{1-n}\right)} \tag{4.3}$$

In this material model, the Young's modulus E is a function of temperature of the cladding, fast neutron fluence, cold work factor and oxygen concentration and is calculated using the MATPRO material model CELMOD. It should be noted that the Young's modulus calculation is done using the MechZry model. So MechZry model is a requirement for the ZryPlasticity model to produce accurate results. The strength coefficient K, strain hardening exponent n and strain rate exponent m are functions of the cladding temperature, fast neutron fluence, fast neutron flux and cold work factor and the expressions for these are given in [35]. To account for the effect of annealing, the Matpro material model CANEAL is used to correct the cold work factor and fast neutron fluence.

To use this model with the return mapping algorithm, the stress after yield needs to be written in terms of the plastic strain (ε_p) instead of the total strain (ε). This can be achieved by substituting σ/E for the elastic strain. Therefore, the stress-plastic strain relation after yield can be written as

$$\varepsilon_p = \left[\frac{\sigma}{K} \left(\frac{10^{-3}}{\dot{\varepsilon}} \right)^m \right]^{\frac{1}{n}} - \frac{\sigma}{E} \tag{4.4}$$

A comparison between the simulated uniaxial test and the experiment is presented in Figure 4.1. Here, a block of Ziracloy with fluence of 10.3 $\times 10^5$ n/m^2 at a temperature of 673 K

is uniaxially pulled at a constant strain rate of 4.17 $\times 10^{-5}$ s^{-1}. The stress-strain curve for this scenario is shown in Figure 4.1. The degradation in the yield stress of the Ziracloy material as a function of temperature is shown in Figure 4.2.

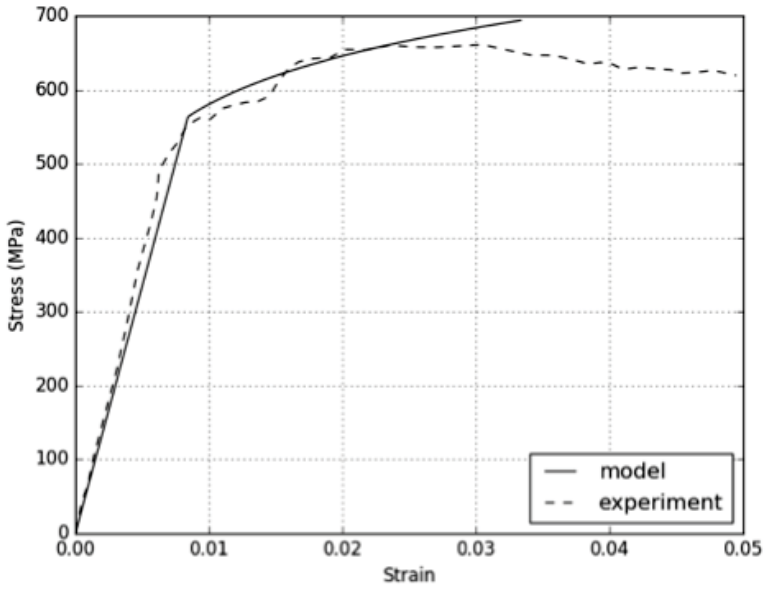

Figure 4.1: Comparison between experiments and simulation for uniaxial test conducted on Ziracloy.

4.2 Cladding Failure (Burst) Criterion

For modeling burst failure of Zircaloy-4 cladding due to microcracking, BISON offers three options:

1. An overstress criterion, which assumes that the time of burst is reached when the local hoop stress equals a limiting burst stress [36]:

$$\sigma_\theta \geq \sigma_b \tag{4.5}$$

where σ_θ (MPa) is the hoop stress and σ_b (MPa) is the burst stress.

2. A plastic instability criterion, which considers cladding burst at the attainment of a limiting value for the effective plastic strain rate:

$$\dot{\varepsilon}_{pl,eff} \geq \dot{\varepsilon_b} \tag{4.6}$$

where $\dot{\varepsilon}_{pl,eff}$ is the effective plastic (creep + plasticity) strain rate and $\dot{\varepsilon_b}$ is the limiting value. Following [37], we choose $\dot{\varepsilon_b} = 100\ h^{-1} \cong 2.78 \cdot 10^{-2}\ s^{-1}$.

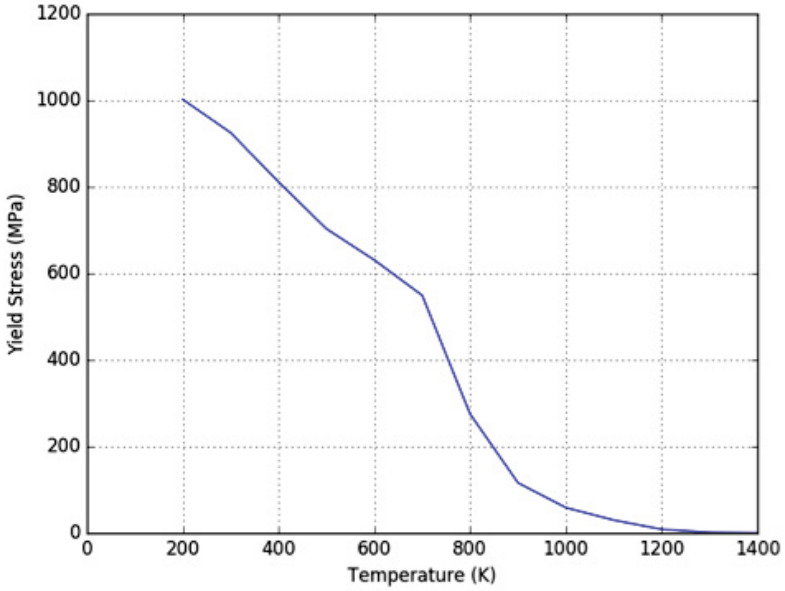

Figure 4.2: Yield stress of Ziracloy material as a function of temperature.

3. A combination of the above criteria, which establishes that cladding burst occurs when either condition 4.5 or 4.6 is fulfilled.

The calculation of the burst stress follows the work of Erbacher et al. [36]. Based on experimental evidence, the burst stress is considered to depend on the temperature and oxygen concentration in the cladding, and is represented by [36]:

$$\sigma_b = a \cdot exp(-bT) \cdot exp\left[-\left(\frac{\eta - \eta_0}{9.5 \cdot 10^{-4}}\right)^2\right] \tag{4.7}$$

where a (MPa) and b (K^{-1}) are constants determined experimentally, and η (-) is the oxygen weight fraction in the cladding. An oxygen weight fraction at fabrication, $\eta_0 = 1.2 \cdot 10^{-3}$, is considered [36]. The current oxygen weight fraction is computed based on the oxygen mass gain from the BISON oxidation model as:

$$\eta = \frac{2r_{cl,o}}{\rho_{Zy} \cdot \left(r_{met,o}^2 - r_{cl,i}^2\right)} \cdot g + \eta_0 \tag{4.8}$$

where $r_{cl,o}$ (m) is the cladding outer radius, ρ_{Zy} = 6550 kg·m^{-3} the density of the cladding metal, $r_{cl,i}$ (m) the cladding inner radius, g (kg·m^{-2}) the oxygen mass, and $r_{met,o} = r_{cl,o} - S/R_{PB}$ with S (m) being the oxide layer thickness and R_{PB}=1.56 the Pilling-Bedworth ratio for Zr. The values for the parameters a and b are given in Table 4.1. In the mixed phase ($\alpha + \beta$) region, linear interpolations of ln(a) and b are made between the values for pure α and middle of $\alpha + \beta$

Table 4.1: Material parameters used to calculate the burst stress of Zircaloy-4 [36].

Phase	a (MPa)	b (K^{-1})
α	830	$1 \cdot 10^{-3}$
50%α 50%β	3000	$3 \cdot 10^{-3}$
β	2300	$3 \cdot 10^{-3}$

(50%α 50%β) phase, and between 50%α 50%β and pure β phase [36]. BISON includes a phase transformation model to compute the volume fractions.

Note that these models have been calibrated using burst data for power ramp rates much slower than those expected in a RIA and thus must be validated against RIA experiments before being used with confidence.

4.3 Time Increment Control

In addition to implementing the new stress-strain relationship as described above, in order to improve the numerical solution in presence of non-linear material behavior (plasticity, creep) during accident situations, a new automatic time step control was developed for BISON. In particular, a time step criterion physically based on the strain rate of the material was implemented. The criterion limits the time step length to guarantee that the increment of strain due to creep during the time step is kept under a pre-defined limiting value:

$$\Delta t \leq \frac{\Delta \varepsilon_{cr,lim}}{\dot{\varepsilon}_{cr}} \tag{4.9}$$

where Δt is the time step length, $\Delta \varepsilon_{cr,lim}$ is the limiting value of creep strain increment, and $\dot{\varepsilon}_{cr}$ is the creep strain rate. As the creep strain rate is different for different locations in the cladding, the most restrictive condition (maximum strain rate across the domain) is considered. This is enforced through a dedicated postprocessor. The new criterion allows for automatic control of the numerical error due to time discretization in presence of non-linear material behavior, thereby guaranteeing a suitable accuracy of the numerical solution. This is important during situations involving high strain rates such as RIA and LOCA accidents. The criterion is combined with the current time step control capability in BISON. A flexible programming structure was set up and in perspective this time stepping method can be extended to incorporate further physically based criteria.

5 OECD RIA Benchmark

5.1 Background and Introduction

In September 2009 the Organization for Economic Co-operation and Development (OECD)/Nuclear Energy Agency (NEA)/Committee on the Safety of Nuclear Installations (CSNI) organized a technical workshop on Nuclear Fuel Behavior during Reactivity Initiated Accidents. One conclusion from a session in the workshop devoted to RIA safety criteria was that fuel rod performance codes are heavily used during the processes of assessing revised safety criteria for the RIA design basis accident. Therefore, as a conclusion of the workshop it was recommended that a benchmark (RIA benchmark Phase I) between fuel performance codes used for assessing RIAs be organized to by the Working Group on Fuel Safety (WGFS).

For the phase I benchmark it was decided to use a set of four experiments on similar highly irradiated fuel rods tested under different conditions. The four experiments were [38]:

- Low temperature, low pressure, stagnant water coolant, very short power pulse (NSRR VA-1)
- High temperature, medium pressure, stagnant water coolant, very short power pulse (NSRR VA-3)
- High temperature, low pressure, flowing sodium coolant, larger power pulse (CABRI CIP0-1)
- High temperature, high pressure, flowing water coolant, medium width power pulse (CABRI CIP3-1)

The results from the RIA benchmark Phase I [38] showed a large variation in many of the thermal and mechanical behavior. In cases with water boiling, there was considerable scatter in cladding temperatures and cladding hoop strain calculations varied by a factor of 10. Therefore as a conclusion of this benchmark, it was recommended to launch a second phase with the following guidelines [39]:

- The emphasis should be put on deeper understanding of the differences in modelling of the different codes; in particular, looking for simpler cases than those used in the first exercise was expected to reveal the main reasons for the observed large scatter in some conditions such as coolant boiling.
- Due to the large scatter between the calculations that was shown in the RIA benchmark Phase I, it appears that an assessment of the uncertainty of the results should be performed

for the different codes. This should be based on a well-established and shared methodology. This also entailed performing a sensitivity study of results to input parameters to assess the impact of initial state of the rod on the final outcome of the power pulse.

Following these guidelines a second phase of the RIA benchmark was launched in early 2014. This benchmark has been organized into two activities [39], namely: 1) To compare the results of different simulations on simplified cases in order to provide additional bases for understanding the differences in modelling of the concerned phenomena and 2) Perform an assessment of the uncertainty of the results, in particular, the impact of the initial states and key models on the results of the transient are investigated.

5.2 Benchmark Specifications

Detailed benchmark specifications were prepared in order to prevent as much as possible the variability between the applied model among the different institutions and codes. The full detailed specifications can be found in [39], but will be summarized below.

Ten cases were defined with an increasing degree of complexity. The first case is focused mainly on the thermal behavior, the second and third cases are focused on the thermo-mechanical behavior, and the fourth through ninth cases added thermal-hydraulic behavior. In the tenth case the thermal and thermal-mechanical models and properties were imposed as close as possible to those used in FRAPTRAN. It was recommended that each code use the standard options for all models. Failure, fuel relocation and oxidation models must be disabled. In order to limit the variability in initial states and properties of high burnup fuel, the cases are limited to a fresh 17x17 PWR type fuel rod described in Figure 5.1. All cases start from ambient conditions and ramp to normal operating conditions during the first 50 seconds and stabilize at those conditions until 100 s, at which point the transient starts. The simulation is concluded at 200 s.

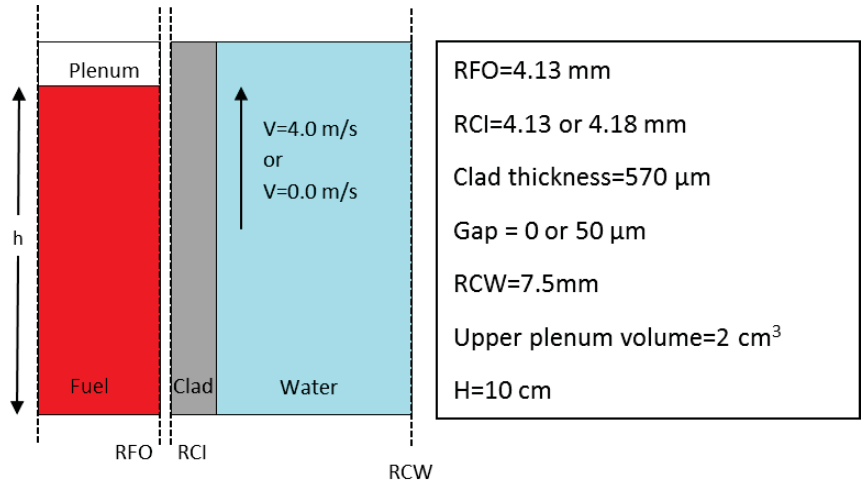

Figure 5.1: Benchmark rod design.

The fuel is composed of standard UO_2 fuel pellets with a diameter of 8.26 mm and a height of 1 cm. No dishing or chamfer is considered in the model. A total fissile column height of 10 cm is specified resulting in a 10 pellet stack. The fuel has a theoretical density of 10970 kg/m^3 with 4% porosity. The cladding is standard Zircaloy-4 material. The fuel rod is initialized with either a 50 μm gap or no gap by modifying the clad inner radius. In nine of the cases the fuel and clad are considered bonded (no slipping occurs) when the fuel is in contact with the cladding. One case allows for perfect slipping between the fuel and the cladding when in contact. The plenum volume is defined as 2 cm^3 and is filled with helium at either a low value (20 bar) or a high value (50 bar) at 20 C.

Depending on the case, the thermal-hydraulic conditions during the transient are:

- PWR Conditions: water coolant at hot zero power (HZP) conditions of 280 C, 155 bar and V = 4.0 m/s
- BWR Conditions: water coolant at cold zero power (CZP) conditions of 20 C, 1 bar and V = 0.0 m/s
- Imposed Conditions: during the first 5 seconds of the transient (100-105 s) a bulk coolant temperature of 300 C with an imposed coolant to clad heat transfer coefficient h = 4,000 W/m^2/K. During all remaining times the bulk coolant temperature is 280 C and h = 40,000 W/m^2/K.
- Fixed Conditions: imposed external clad temperature of 280 C and external pressure of 155 bar

The power pulse will start from zero power at t = 100s and is approximated with a triangular shape. The pulse width will be 30 ms full width at half max (FWHM). Two maximum powers will be defined, a low value to avoid departure from nucleate boiling (DNB) and a high value to make DNB possible. For the PWR cases the low value will be 0.4 MW which for the 30 ms FWHM triangular pulse will result in 50.82 cal/g of injected energy into the fuel rod. The PWR high value will be 1.0 MW resulting in 127.06 cal/g. For BWR cases the low value will be 0.3 MW (38.12 cal/g) and 1.0 MW (127.06 cal/g). All the power is injected into the UO_2 and no contribution will be released in the cladding or coolant. The radial and axial profiles in the fuel are required to be flat. All ten cases are summarized in Figure 5.2. The required parameters to be calculated are outlined in Figure 5.3.

5.3 BISON Model

The geometry described in Figure 5.1 was interpreted into a 2D-RZ model for BISON. Owing to the simplicity of the model specified in the benchmark the internal BISON module (SmearedPelletMesh) was used to generate the mesh. The fuel was defined with 10 radial mesh elements and 40 axial elements. The cladding was defined with 5 radial elements and 40 axial elements. The cladding height was defined to achieve a plenum volume of 2 cm^3. The geometry is shown in Figure 5.4.

		Geometry		Contact Conditions		Thermomechanical Models		Thermal Hydraulic Conditions				Maximum Power		Helium Pressure	
		No gap	Open gap	No Slipping	Slipping	Standard	Imposed	Fixed	PWR	BWR	Imposed	Low	High	Low	High
Thermal	**case 1**	X		X		X		X					X	X	
Mechanical	**case 2**		X	X		X		X					X	X	
	case 3		X		X	X		X					X	X	
	case 10		X	X			X	X					X	X	
Thermal Hydraulic	**case 6**	X		X		X				X		X		X	
	case 7	X		X		X				X			X	X	
	case 4	X		X		X			X			X		X	
	case 5	X		X		X			X				X	X	
	case 8	X		X		X			X				X		X
	case 9	X		X		X					X		X	X	

Figure 5.2: Summary of benchmark cases.

The fuel is assumed elastic with a Young's Modulus of 200 GPa, a Poisson ratio of 0.345 and thermal expansion coefficient as defined in MATPRO. The thermal properties of the fuel are defined using the built-in ThermalFuel module with a porosity of 0.04. The transient power pulse is applied to the fuel as a uniform heat source using the HeatSource module in the BISON Kernels block.

The cladding is modeled using the SolidModel module with the Young's Modulus applied as a function of temperature and a Poisson ratio of 0.3. The thermal properties were defined with the ThermalZry module and the thermal expansion coefficient was applied as a function of temperature from MATPRO. An IsotropicPlasticity module was also applied to the cladding to capture the effect of instantaneous plasticity resulting from the rapid expansion of the fuel into the cladding due to thermal expansion. The yield strength of the cladding was defined as a function of temperature from [35]. No creep models were used due to the small time scales involved in RIA transients.

For cases 4, 5 and 8 that specify PWR Conditions for the thermal-hydraulic conditions the CoolantChannel module in BISON was used. Cases 1, 2, and 3 used a fixed temperature on the outside of the cladding. Case 9 required imposed conditions for the bulk coolant temperature and the convective heat transfer coefficient. This case used the ConvectiveFluxFunction boundary condition with the appropriate temperature and heat transfer coefficient defined above.

Cases 6, 7 and 10 were not completed for this benchmark. Cases 6 and 7 are for BWR CZP conditions which imposes a coolant velocity of 0.0 m/s. The BISON CoolantChannel module is not currently applicable for these conditions. Case 10 required modifying all material thermal and mechanical models to match those of FRAPTRAN. Due to time constraints this was not performed.

Parameter	Unit	Description
EDR	cal/g	Energy Injected in the whole rodlet as a function of time
DHR	cal/g	Variation of radial average enthalpy with respect to initial conditions of the transient in the rodlet as a function of time (at z=h/2) (please note that: DHR(t=0)=0)
TFC	°C	Temperature of fuel centerline as a function of time (at z=h/2)
TFO	°C	Temperature of fuel outer surface as a function of time (at z=h/2)
TCI	°C	Temperature of clad inner surface as a function of time (at z=h/2)
TCO	°C	Temperature of clad outer surface as a function of time (at z=h/2)
ECMH	%	Clad mechanical (elastic + plastic) hoop strain at the outer part of the clad as a function of time (at z=h/2)
ECMZ	%	Clad mechanical (elastic + plastic) axial strain at the outer part of the clad as a function of time (at z=h/2)
ECTH	%	Clad total (thermal + elastic + plastic) hoop strain at the outer part of the clad as a function of time(at z=h/2)
ECTZ	%	Clad total (thermal + elastic + plastic) axial strain at the outer part of the clad as a function of time(at z=h/2)
ECT	mm	Clad total axial elongation as a function of time
EFT1	mm	Fuel column total axial elongation as a function of time
EFT2	mm	Fuel column thermal axial elongation as a function of time
SCH	MPa	Clad hoop stress at outer part of the clad as a function of time (at z=h/2)
SCZ	MPa	Clad axial stress at outer part of the clad as a function of time (at z=h/2)
RFO	mm	Fuel outer radius as a function of time (at z=h/2)
RCI	mm	Clad inner radius as a function of time (at z=h/2)
HFC	$W/m^2/K$	Fuel to clad heat transfer coefficient as a function of time (at z=h/2)
HCW	$W/m^2/K$	Clad to water heat transfer coefficient as a function of time (at z=h/2)
PG	bar	Free volume pressure as a function of time
VOL	mm^3	Free Volume as a function of time (including open porosity)

Figure 5.3: Output parameters required for the benchmark.

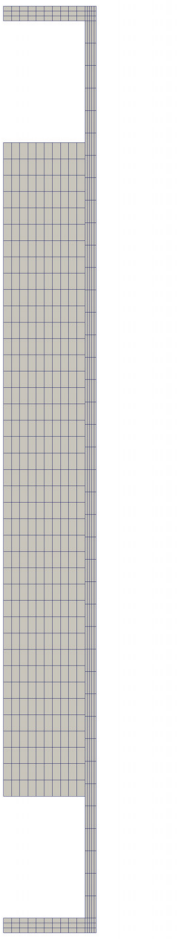

Figure 5.4: BISON fuel rod geometry and mesh. Representation is magnified 3X in the radial direction for clarity.

5.4 Results

A complete compilation of all the results for all cases and codes has been compiled by the OECD [40] comparing each output parameter listed in Figure 5.3. Additionally a more detailed comparison was performed between BISON and FRAPTRAN [41] on prior results before improvements were made to the cladding plasticity model. This report will present and compare the updated results of BISON and FRAPTRAN simulations for case 5 of the benchmark.

An important parameter to consider when discussing RIA transients is the amount of energy injected into the fuel and the resulting fuel radial average enthalpy. Historically the US Nuclear Regulatory Commissions (USNRC) acceptance criterion for reactivity excursions has been based upon the maximum radial average fuel enthalpy in the fuel rod [42]. Therefore, for safety considerations it is necessary to be able to accurately model the fuel radial average enthalpy of the rodlet. The first two parameters of interest in Figure 5.3 were the energy injected into the rodlet and the variation of radial average enthalpy from the starting conditions at time zero. The energy injected, fuel radial average enthalpy, and power pulse are shown in Figure 5.5. Figure 5.6 shows the fuel radial average enthalpy over a longer duration to show the good agreement between the two codes. Good agreement on the radial average enthalpy of the fuel shows that both codes are calculating comparable radial profiles throughout the fuel pellet during the entire simulation.

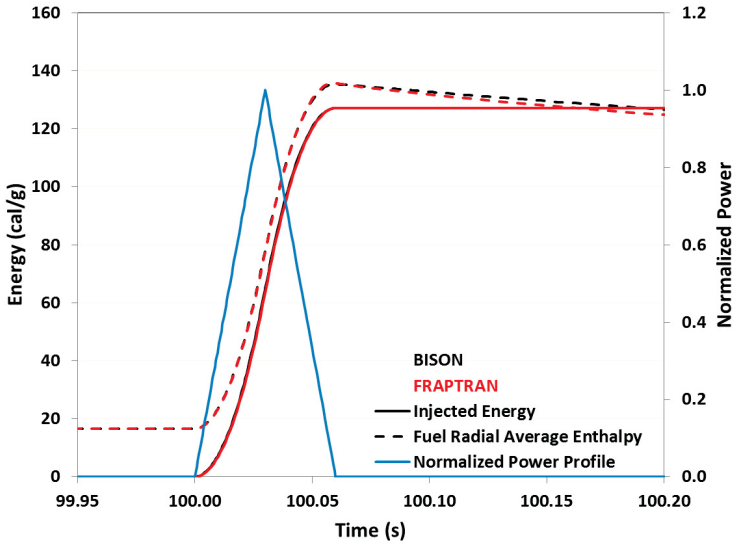

Figure 5.5: Profile comparisons between FRAPTRAN and BISON for the energy injected into the rodlet and fuel radial average enthalpy shown with the simplified 30 ms FWHM power profile.

The temperature profiles at different radial locations in the rodlet are shown in Figure 5.7. The fuel centerline temperature shows good agreement between the two codes over the entire transient. The fuel surface and cladding surface temperatures deviate slightly between the two codes. Due to the complexity of the problem and the multiphysics simulation involved it is

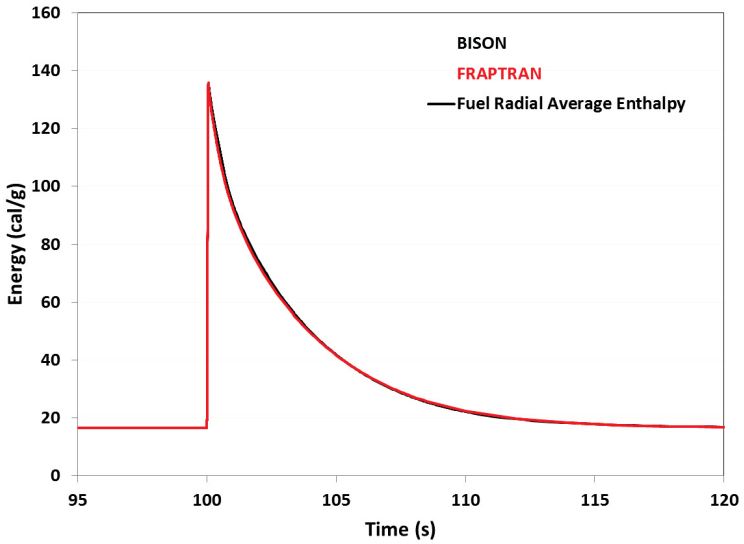

Figure 5.6: Fuel radial average enthalpy shows excellent agreement between BISON and FRAPTRAN.

difficult to pinpoint the cause of the temperature differences between the two codes. There are large variations between the fuel to cladding gap conductance and cladding to coolant heat transfer coefficient between the two codes that will cause differences in temperatures. Also, differences in mechanical models have effects on various mechanisms that affect the energy transport, such as the gap width between the fuel and cladding.

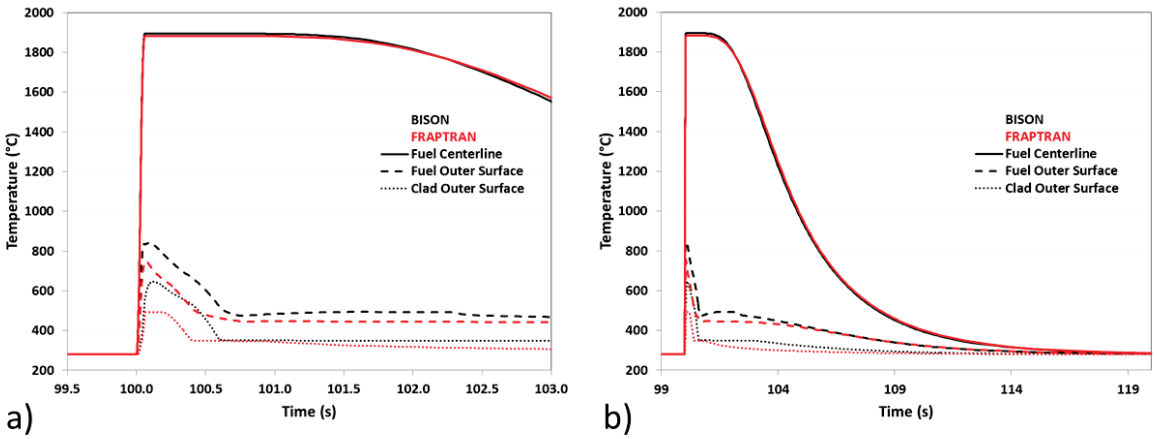

Figure 5.7: Temperature profiles at different radial locations on the rodlet. a) Temperature profiles during a smaller temporal scale around the power pulse and b) larger temporal scale showing temperature profiles during the cooling of the rodlet.

The combination of such a large and rapid temperature increase and the fuel having a coefficient of thermal expansion twice that of the cladding, results in large hoop strains being applied to the cladding. The hoop strain and corresponding hoop stress at the outer surface of the cladding are shown in Figure 5.8. During a RIA event the cladding is forced to expand and conform to the expansion of the fuel, therefore the cladding undergoes a displacement controlled problem. The cladding total hoop strain is controlled by the radial expansion of the fuel until separation occurs during cooling. As such, the total hoop strain shows some variation between the codes. They have very similar evolutions, but FRAPTRAN predicts approximately 0.4% more strain than BISON after the pulse. This variation correlates to a difference in the maximum outer radius, 4.209 mm in BISON and 4.219 mm in FRAPTRAN. This is likely due to multiple reasons. First, FRAPTRAN assumes a rigid pellet that cannot yield, while BISON assumes a compliant fuel pellet. Also differences in fuel thermal expansion and plasticity models between codes could result in the variations in calculated strain.

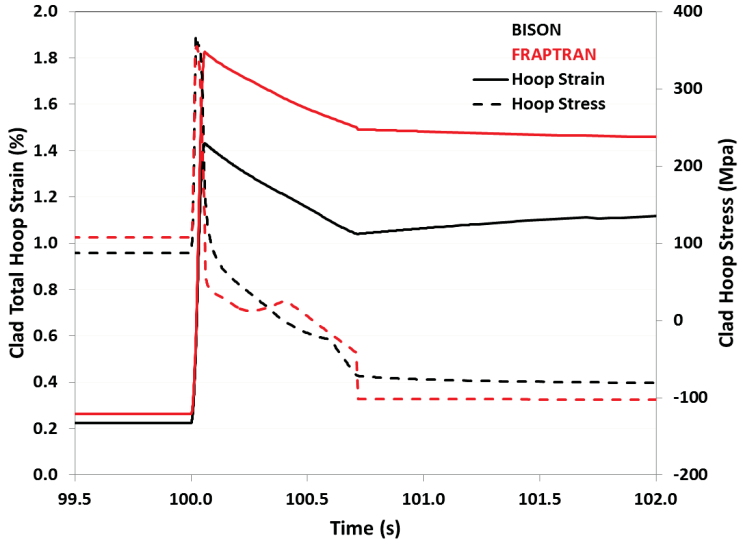

Figure 5.8: Hoop stress and total hoop strain at the outer surface of the claddingTemperature profiles at different radial locations on the rodlet.

Each code predicted a maximum hoop stress of approximately 340 MPa and were within 20 MPa of each other throughout the transient. The two codes agree reasonably well on the stress, except for a short time just after the power pulse. During this time just after the pulse (100.06-101.0s) there is a complicated trade-off between elastic strain and the development of plastic strain. The increase in plastic strain is due to the decrease of the Zircaloy yield strength as the temperature increases. The temperature dependent yield strength capability described in Section 4.1 was added to BISON as a result of participation in this OECD benchmark.

5.5 Summary

The objective of the first task in Phase II of the RIA benchmark was to compare the results of different simulations on ten simplified cases in order to better understand the differences in modelling of the concerned phenomena. INL was able to participate in this international collaboration and contribute to seven of the ten cases for the benchmark. The complete results are compiled in an OECD/NEA/CSNI report. The results for case 5 of the benchmark have been compared more rigorously with the results obtained from the USNRC using FRAPTRAN. In general, the results compare reasonably well in both thermal and mechanical aspects, and differences can likely be explained by variations in thermal and mechanical models applied to the materials.

6 Verification and Validation

6.1 Verification

"Verification must precede Validation.... Attempting to validate a model using a code that may still contain (serious) errors can lead to a false conclusion about the validity of the model" [43]. In other words, verification is a prerequisite to validation.

Essentially, verification ensures that each piece of code performs as expected and is the foundation upon which a strong validation basis is built. To that end, considerable emphasis has been placed on verification in BISON. Referencing Roache [44], Oberkampf [45] points out that verification has two components, referred to as code and solution verification. Strongly influenced by Oberkampf's work, in this report we refer to code verification as the mathematical correctness of the code implementation and solution verification as a quantitative assessment of the numerical accuracy of a given solution to a particular problem.

6.1.1 Code Verification

Code verification is here considered in terms of software engineering practices, unit testing and regression testing.

Software Engineering

"Often verification and validation are parts of an overarching software quality assurance (SQA) program. SQA methods are enacted to guide the software development cycle and may include recommendations or requirements for software engineering tasks such as gathering and recording customer requirements, using revision control software, writing code, testing the software, documenting the software, and releasing the application, among others. It is common to measure the quality of the software development process by assessing how well the development team is fulfilling the requirements in each of these areas" [46].

The BISON software is kept in a Gitlab version control repository at INL. The MOOSE software is open-source and maintained in a similar version control repository know as Github. The BISON unit and regression tests, example problems, validation cases and documentation are maintained in the same BISON Gitlab repository. This enables traceability of each code, validation case or documentation change. The author, date, and details of the changes are recorded with each commit to Gitlab and Github. It is also possible to retrieve a copy of the software from any point in its history. Through the use of revision control software, developers are able to maintain the current copy of BISON on their local machines and make frequent changes to BISON without fear of undoing another's changes or of making irrecoverable changes.

The BISON team relies on software configuration management tools and practices set up for MOOSE applications. Continuous integration is also accomplished through Gitlab. With each commit to BISON (or any MOOSE-based component), Gitlab automatically compiles the software across multiple computer platforms. If the compilation process is successful, the new version of the software runs the complete set of regression tests. This also happens on multiple computer platforms. This continuous integration, as it is called, helps ensure that the regression tests run correctly at all times. If a commit causes a test to fail, the failure is immediately noted through an electronic message to the developers who then correct the error.

In addition to the testing that occurs with each commit, code coverage data is also automatically produced. This information includes line and function coverage at the file, directory, and library level. The development team regularly reviews this information to ensure that the code coverage remains high.

All of this information (commit history and details, build status, test status, and code coverage) is available at the BISON Gitlab site and is thus easily available to developers and others.

As mentioned above, the BISON team maintains its documentation in the same Gitlab Repository that holds the application software. The documentation includes a user manual [19], a theory manual [18], an assessment document [47], a publication list or bibliography, and a set of workshop or training presentation slides.

As BISON continues to develop and mature, it is anticipated that a formal assessment of its software quality practices will occur (using, e.g., ASME NQA-1, CMMI, or ISO 9000 standards and models). It is worth noting that MOOSE has received ASME NQA-1 certification.

Unit Testing

Code verification ensures that a model represented in computer code calculates the correct results as defined by the mathematical definition of the model. Verification is accomplished through tests, specially designed, that exercise a particular feature of a given model. As an example, for heat conduction, we can verify that the finite element solution of a linear temperature field is in fact linear even when the mesh is composed of irregular elements. For solid mechanics, we can test that the proper stress field results when a uniform pressure is applied.

By way of example, consider the process followed to introduce a new thermal conductivity model for UO_2 fuel. Having identified the particular form of the model (the mathematical description), the developer can identify the inputs to the model (e.g., temperature) as well as the outputs (thermal conductivity). The developer creates a test that will exercise the new model. This test will require specific boundary conditions and perhaps other carefully controlled inputs in order to produce the exact results expected through an independent, analytic calculation.

The developer must of course also encode the relevant equations in the BISON software and compile the new code. Having done so, the developer exercises the new capability on the new test. If the computed thermal conductivity does not match the analytic expression, the developer searches for errors in the code and in the test until the discrepancy is resolved. Note that more than one verification test may be, and often is, required to give confidence that the encoded model is mathematically correct.

It should be understood that much of the underlying software in use by BISON has its own set of verification tests. In particular, verification tests concerned with the correctness of the finite

element formulation are maintained at the MOOSE and libMesh levels.

BISON has many verification tests, checking solid mechanics, heat conduction, gap heat transfer, material models, mechanical contact, thermal contact, large strain capabilities, boundary conditions, plenum pressure determination, output, and many other phenomena needed for nuclear fuel analysis. That these tests run properly is evidence that the models have been implemented correctly. BISON SQA processes require that all new code committed to the repository is supported by adequate unit testing.

A review of several of BISON's verification tests, along with an overview of verification in the context of nuclear fuel performance software in general and of BISON in particular, is in [46].

Regression Testing

As a matter of engineering practice, BISON developers are responsible for developing regression tests for all of the code they develop. This helps ensure that future code changes do not break existing functionality. Some tests exercise the interaction of various models, and many others are single-feature verification tests.

6.1.2 Solution Verification

Solution verification ensures that all validation simulations are adequately resolved in terms of spatial and temporal discretization, and all accompanying iterative solutions are sufficiently converged. This is a very large task given that the BISON validation cases for LWR fuel are expected to number in the hundreds. Since most LWR problems share similar geometry, materials and loading conditions, a first and substantial step will be to develop a representative LWR fuel rod problem for which solution verification is demonstrated. Note that, eventually, solution verification will be conducted for each of the challenge problems identified above. The current status of a representative solution verification analysis is outlined below.

Typical LWR Fuel Rod Problem

To quantitatively evaluate the numerical accuracy of BISON validation problems, simulations with representative validation-problem features were spatially and temporally resolved and the results compared. These representative features are: loading (i.e., power supplied to the fuel, coolant pressure on the cladding), boundary conditions, geometry, mesh, and material models. A typical power history was assumed as shown in Figure 6.1. Note that this power history is not a discrete series of powers for specified durations, as may be common for older fuel performance codes. It is, rather, a continuous function of time. The boundary conditions that represent coolant temperature and pressure were typical for a pressurized water reactor.

The spatial resolution simulations consisted of four levels of mesh refinement, which are summarized in Table 6.1. Figure 6.2 shows a mesh with refinement level C, which is the typical mesh density used in BISON LWR validation work.

The figures of merit in this resolution study are parameters that are important to all validation simulations, which are: power, fuel centerline temperature (FCT), fission gas release (FGR), and rod diameter. As defined here, power is the total nuclear power obtained by integrating the

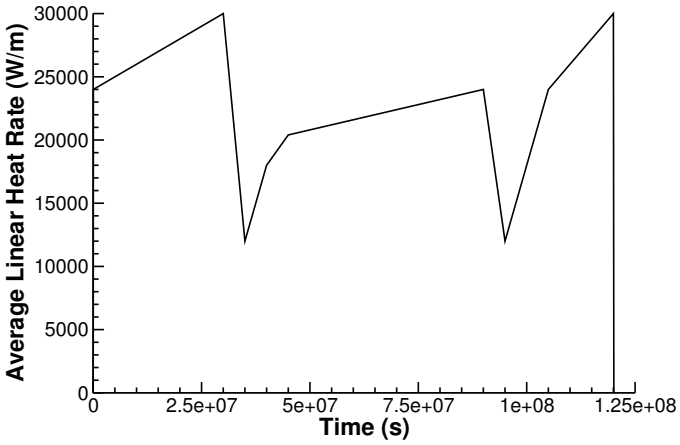

Figure 6.1: Representative power history used for the spatial and temporal solution verification studies.

Table 6.1: The number and aspect ratios of the elements used in the various meshes in the solution verification study.

Mesh	A	B	C	D
No. Axial Elements Fuel	275	550	550	1375
No. Radial Elements Fuel	3	6	12	22
No. Axial Elements Clad	281	556	556	813
No. Radial Elements Clad	1	3	4	5
Aspect Ratio Fuel	9.85	9.85	19.70	14.45
Aspect Ratio Clad	22.19	33.29	44.38	37.53

volumetric fission rate over the entire fuel volume. Figure 6.3 shows relative error calculations from these figures of merit, where results from refinement level D are the basis for relative error calculations. For the parameters of interest, the estimated spatial error using the typical validation mesh (Mesh C) is on the order of 1% or less, which is adequate for validation studies. Note that power has a larger relative error than the other quantities considered. Power is more sensitive to mesh refinement due to the steep gradient in the radial power profile near the pellet periphery.

Figure 6.4 shows results from the temporal resolution study. The mesh with refinement level C was used for these calculations, where the number of times steps was increased and the relative error calculation is with respect to the simulation with the greatest number of times steps. The acceptable number of time steps was determined by decreasing time step size (i.e. increasing the total number of time steps) and observing the relative error and the change in relative error. In this case, the relative error is very small even for the lowest number of time steps. Therefore, time resolution is adequate in all cases.

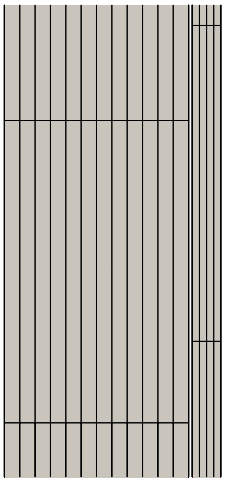

Figure 6.2: Illustration of a section of mesh C showing the radial and axial element sizes. Mesh C is representative of the mesh used for all validation cases used in this study.

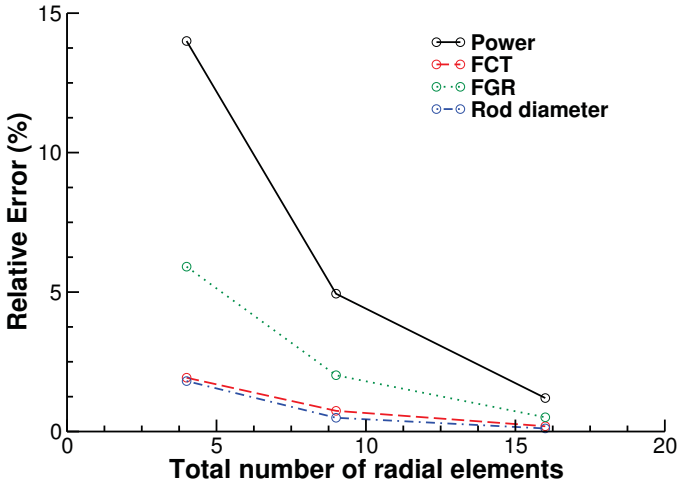

Figure 6.3: Spatial resolution results for the solution verification study. Relative percent error is presented for four metrics of interest: Power, FCT, FGR, and rod diameter as a function of the total number of radial elements in the mesh. The relative error is with respect to the finest mesh studied, Mesh D.

6.2 Validation

BISON is also being expanded to include simulation of Reactivity Insertion Accident (RIA) behavior. As indicated above, from its beginning BISON was designed to handle transient thermal behavior, including very rapid transients. The code also includes a large-strain mechanics formulation, essential to correctly analyze high cladding deformation during RIAs. Further, many of the high temperature material models required for accident analysis have already been

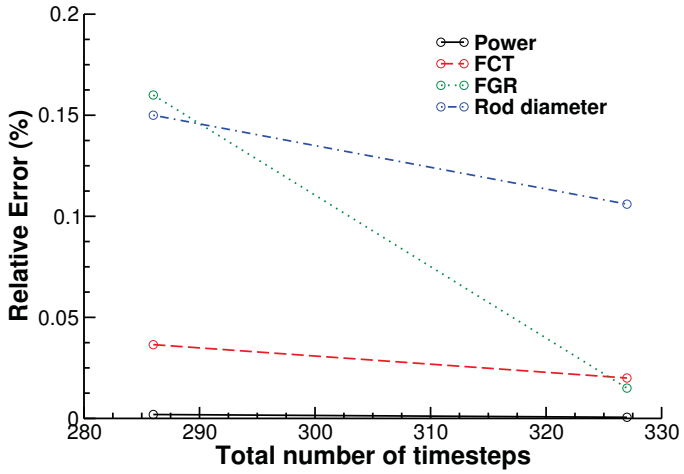

Figure 6.4: Temporal resolution results for the solution verification study. Relative percent error is presented for four metrics of interest: Power, FCT, FGR, and Rod diameter as a function of the total number time steps taken in the simulation. The relative error is with respect to the case with the most time steps, 681.

implemented.

6.2.1 Current Validation Status

There have been no BISON comparisons to RIA experiments to date. Noteworthy, however, is INL's participation in the second OECD benchmark focused on simulating RIA behavior using fuel performance codes, as described above. Results from the earlier first benchmark exercise demonstrated a large amount of scatter in the predictions from various codes, thus the second benchmark included simpler cases and was designed to provide a deeper understanding of the differences in modeling between the codes. The second benchmark includes ten cases that initially isolate transient thermal behavior and then gradually increase in complexity by including mechanical effects and thermal hydraulic behavior. BISON has been run on most of the cases and compared to several other fuel performance codes. Specific comparisons between BISON and FRAPTRAN show reasonable agreement between the codes, particularly the transient thermal behavior [41]. A second phase of the benchmark will include RIA sensitivity and uncertainty analysis.

6.2.2 Planned Validation Work

Table 6.2 identifies experiments that are planned for use in validation of RIA behavior in BISON. The experiments are listed roughly in the order that they will be addressed. Note that this set of experiments was recommended in the CASL RIA Challenge Problem Implementation Plan [2].

It is anticipated that more RIA cases will be included as experience is gained with RIA simulation and potential code deficiencies are identified.

Table 6.2: Planned RIA experiments for BISON validation.

Experiment	Rod/Test	Description
CABRI	Na-2	PWR 17x17 fuel at 33 MWd/kgU, Na coolant, 9.5 μs pulse, 220 cal/g max enthalpy
CABRI	Na-3	PWR 17x17 fuel at 52 MWd/kgU, Na coolant, 9.5 μs pulse, 138 cal/g max enthalpy
CABRI	Na-5	PWR 17x17 fuel at 64 MWd/kgU, Na coolant, 9.1 μs pulse, 113 cal/g max enthalpy
CABRI	Na-10	PWR 17x17 fuel at 64 MWd/kgU, Na coolant, 31 μs pulse, 112 cal/g max enthalpy
NSRR	VA1	PWR 17x17 fuel at 71 MWd/kgU, ZIRLO clad, $\approx$5 μs pulse, 133 cal/g max enthalpy
NSRR	VA2	PWR 17x17 fuel at 77 MWd/kgU, MDA clad, $\approx$5 μs pulse, 130 cal/g max enthalpy
NSRR	VA3	PWR 17x17 fuel at 71 MWd/kgU, ZIRLO clad, $\approx$5 μs pulse, 108 cal/g max enthalpy
NSRR	VA4	PWR 17x17 fuel at 77 MWd/kgU, MDA clad, $\approx$5 μs pulse, 109 cal/g max enthalpy

7 Summary and Conclusions

Fuel performance capabilities required to address the CASL RIA challenge problem have been identified and the current status of BISON in each of these areas has been outlined. Important enhancements to BISON for accident analysis have recently been completed and reported herein. Much of the required capability for RIA analysis is in place. Key capability gaps identified in this report include:

- Assessment of and potential calibration of the existing fission gas burst release model to RIA behavior
- Assessment of and potential calibration of the existing clad burst model to RIA behavior
- Code enhancements to permit discrete fracture analysis of cladding
- Inclusion of the effects of hydrides on cladding mechanical behavior
- Assessment of the importance of CRUD to RIA analysis

BISON has been successfully applied to a variety of cases from the current OECD RIA benchmark exercise, with good comparisons to the FRAPTRAN fuel accident analysis code.

Although significant BISON validation to LWR fuel has been completed, there have been no comparisons to RIA behavior. For BISON to be used with confidence for the RIA challenge problem, this must become a priority. This validation effort will likely identify additional areas where code development is needed.

Bibliography

[1] G. B. Swindlehurst. Challenge problem charter: Reactivity initiated accident. Technical Report CASL-I-2013-0059-002, Consortium for Advanced Simulation of LWRs, 2016.

[2] G. B. Swindlehurst. Challenge problem implementation plan: Reactivity initiated accident. Technical Report CASL-I-2013-0060-003, Consortium for Advanced Simulation of LWRs, 2016.

[3] R. L. Williamson, J. D. Hales, S. R. Novascone, M. R. Tonks, D. R. Gaston, C. J. Permann, D. Andrs, and R. C. Martineau. Multidimensional multiphysics simulation of nuclear fuel behavior. *J. Nucl. Mater.*, 423:149–163, 2012.

[4] J. D. Hales, R. L. Williamson, S. R. Novascone, D. M. Perez, B. W. Spencer, and G. Pastore. Multidimensional multiphysics simulation of TRISO particle fuel. *J. Nucl. Mater.*, 443:531–543, 2013.

[5] Pavel Medvedev. Fuel performance modeling results for representative FCRD irradiation experiments: Projected deformation in the annular AFC-3A U-10Zr fuel pins and comparison to alternative designs. Technical Report INL/EXT-12-27183 Revision 1, Idaho National Laboratory, 2012.

[6] N. N. Carlson, C. Unal, and J. D. Galloway. Formulation of the constituent distribution model implemented into the BISON framework for the analysis of performance of metallic fuels with some initial simulation results. Technical Report LA-UR-13-26824, Los Alamos National Laboratory, 2013.

[7] Pavel Medvedev. Summary report on the fuel performance modeling of the AFC-2A, 2B irradiation experiments. Technical Report INL/EXT-13-30006, Idaho National Laboratory, 2013.

[8] K. E. Metzger, T. W. Knight, and R. L. Williamson. Model of U_3Si_2 fuel system using BISON fuel code. In *Proceedings of the International Congress on Advances in Nuclear Power Plants - ICAPP 2014*, Charlotte, NC, April 6–9 2014.

[9] D. Gaston, C. Newman, G. Hansen, and D. Lebrun-Grandié. MOOSE: A parallel computational framework for coupled systems of nonlinear equations. *Nucl. Eng. Design*, 239:1768–1778, 2009.

[10] D. A. Knoll and D. E. Keyes. Jacobian-free Newton-Krylov methods: a survey of approaches and applications. *J. Comput. Phys.*, 193(2):357–397, 2004.

[11] J. D. Hales, S. R. Novascone, R. L. Williamson, D. R. Gaston, and M. R. Tonks. Solving nonlinear solid mechanics problems with the Jacobian-free Newton Krylov method. *CMES: Comput. Model. Eng. Sci.*, 84(2):123–154, 2012.

[12] G. Pastore, L. Luzzi, V. Di Marcello, and P. Van Uffelen. Physics-based modelling of fission gas swelling and release in UO_2 applied to integral fuel rod analysis. *Nucl. Engrg. Design*, 256:75–86, 2013.

[13] A. M. Ross and R. L. Stoute. Heat transfer coefficient between UO_2 and Zircaloy-2. Technical Report AECL-1552, Atomic Energy of Canada Limited, 1962.

[14] J. D. Hales, D. Andrs, and D. R. Gaston. Algorithms for thermal and mechanical contact in nuclear fuel performance analysis. In *Proceedings of the International Conference on Mathematics and Computational Methods Applied to Nuclear Science and Engineering*, Sun Valley, Idaho, May 5-9, 2013.

[15] Benjamin S. Kirk, John W. Peterson, Roy H. Stogner, and Graham F. Carey. libMesh: A C++ library for parallel adaptive mesh refinement/coarsening simulations. *Engineering with Computers*, 22(3-4):237–254, January 2006.

[16] Portable, extensible toolkit for scientific computation. http://www.mcs.anl.gov/petsc/. Retrieved April 25, 2012.

[17] Robert D. Falgout and Ulrike Meier Yang. HYPRE: A library of high performance preconditioners. In *International Conference on Computational Science (3)*, pages 632–641, 2002.

[18] J. D. Hales, R. L. Williamson, S. R. Novascone, G. Pastore, B. W. Spencer, D. S. Stafford, K. A. Gamble, D. M. Perez, R.J. Gardner, and W. Liu. BISON theory manual: The equations behind nuclear fuel analysis. Technical Report INL/EXT-13-29930, Rev.2, Idaho National Laboratory, September 2015.

[19] J. D. Hales, K. A. Gamble, B. W. Spencer, S. R. Novascone, G. Pastore, W. Liu, D. S. Stafford, R. L. Williamson, D. M. Perez, and R. J. Gardner. BISON users manual. Technical Report INL/MIS-13-30307, Rev. 3, Idaho National Laboratory, September 2015.

[20] K. Lassmann, C. O'Carroll, J. van de Laar, and C. T. Walker. The radial distribution of plutonium in high burnup UO_2 fuels. *J. Nucl. Materials*, 208:223–231, 1994.

[21] D. D. Lanning and C. R. Hann. Review of methods applicable to the calculation of gap conductance in zircaloy-clad uo2 fuel rods. Technical Report BWNL-1894, UC-78B, 1975.

[22] M.W. Heinstein and T.A. Laursen. An algorithm for the matrix-free solution of quasistatic frictional contact problems. *Internat. J. Numer. Methods Engrg.*, 44(9):1205–1226, 1999.

[23] J. K. Fink. Thermophysical properties of uranium dioxide. *J. Nucl Materials*, 279(1):1–18, 2000.

[24] P.G. Lucuta, Hj. Matzke, and I.J. Hastings. A pragmatic approach to modelling thermal conductivity of irradiated UO_2 fuel: Review and recommendations. *Journal of Nuclear Materials*, 232(2–3):166–180, 1996.

[25] A. Marion (NEI) letter dated June 13, 2006 to H. N. Berkow (USNRC/NRR). Safety Evaluation by the Office of Nuclear Reactor Regulation of Electric Power Research Institute (EPRI) Topical Report TR-1002865, Topical Report on Reactivity Initiated Accidents: Bases for RIA Fuel rod Failures and Core Coolability Criteria. http://pbadupws.nrc.gov/docs/ML0616/ML061650107.pdf, 2006.

[26] Y. R. Rashid. Mathematical modeling and analysis of fuel rods. *Nuclear Engineering and Design*, 29:22–32, 1974.

[27] R. L. Williamson and D. A. Knoll. Simulating dynamic fracture in oxide fuel pellets using cohesive zone models. In *20th International Conference on Structural Mechanics in Reactor Technology (SMiRT 20)*, Espoo (Helsinki), Finland, August 9–14 2009.

[28] B. W. Spencer, H. Huang, J. Dolbow, and J. D. Hales. Discrete modeling of early-life thermal fracture in ceramic nuclear fuel. In *2014 LWR Fuel Performance Meeting – TopFuel*, Sendai, Japan, September 14–17 2014.

[29] G. Pastore, D. Pizzocri, J. D. Hales, S. R. Novascone, D. M. Perez, B. W. Spencer, R.L. Williamson, P. Van Uffelen, and L. Luzzi. Modelling of transient fission gas behaviour in oxide fuel and application to the BISON code. In *Enlarged Halden Programme Group Meeting, Røros, Norway, September 7-12*, 2014.

[30] M. Limbäck and T. Andersson. A model for analysis of the effect of final annealing on the in- and out-of-reactor creep behavior of zircaloy cladding. In *Zirconium in the Nuclear Industry: Eleventh International Symposium*, ASTM STP 1295, pages 448–468, 1996.

[31] N. E. Hoppe. Engineering model for zircaloy creep and growth. In *Proceedings of the ANS-ENS International Topical Meeting on LWR Fuel Performance*, pages 157–172, Avignon, France, April 21-24, 1991.

[32] Y. Rashid, R. Dunham, and R. Montgomery. Fuel analysis and licensing code: FALCON MOD01. Technical Report EPRI 1011308, Electric Power Research Institute, December 2004.

[33] P. M. Gilmore, H. H. Klepfer, and J. M. Sorensen. EPRI PWR fuel cladding corrosion (PFCC) model volume 1: Theory and users manual. Technical Report TR-105387-V1, December 1995.

[34] D.S. Stafford. Multidimensional simulations of hydrides during fuel rod lifecycle. *Journal of Nuclear Materials*, 466:362 – 372, 2015.

[35] K. J. Geelhood, C. E. Beyer, and W. G. Luscher. PNNL stress strain correlation for Zircaloy. Technical Report PNNL-17700, Pacific Northwest National Laboratory, 2008.

[36] F. J. Erbacher, H. J. Neitzel, H. Rosinger, H. Schmidt, and K. Wiehr. Burst criterion of Zircaloy fuel claddings in a loss-of-coolant accident. In *Zirconium in the Nuclear Industry, Fifth Conference, ASTM STP 754, D.G. Franklin Ed.*, pages 271–283. American Society for Testing and Materials, 1982.

[37] V. Di Marcello, A. Schubert, J. van de Laar, and P. Van Uffelen. The TRANSURANUS mechanical model for large strain analysis. *Nuclear Engineering and Design*, 276:19–29, 2014.

[38] RIA fuel codes benchmark. Technical Report NEA/CSNI/R(2013)7, NEA, OCED, 2013.

[39] Reactivity Insertion Accident (RIA) fuel codes benchmark phase-II report - Volume 2: Task No. 1 specifications. Technical Report NEA/CSNI/R(2016)6, NEA, OCED, 2016.

[40] Reactivity Insertion Accident (RIA) fuel codes benchmark phase-II report - Volume 1: Simplified cases results, Summary and analysis. Technical Report NEA/CSNI/R(2016)6, NEA, OCED, 2016.

[41] C. Folsom, P. Raynaud, A. Zabriskie, R. Williamson, H. Ban, and D. Wachs. Case comparison between FRAPTRAN and BISON for an idealized RIA of a light water reactor. In *American Nuclear Society Winter Meeting*, Washington DC, 8–12 November 2015.

[42] Assumptions used for evaluating a control rod ejection accident for pressurized water reactors. Technical Report Regulatory Guide 1.77, US Atomic Energy Commission, 1974.

[43] L. E. Schwer. An overview of the PTC 60/V&V 10: Guide for verification and validation in computational solid mechanics. *Engrg. Comput.*, 23:245–252, 2007.

[44] P. J. Roache. *Verification and Validation in Computational Science and Engineering*. Hermosa Publishers, Albuquerque, NM, 1998.

[45] W. L. Oberkampf and T. G. Trucano. Verification and validation benchmarks. *Nucl. Engrg. Design*, 238(3):716–743, 2008.

[46] J. D. Hales, S. R. Novascone, B. W. Spencer, R. L. Williamson, G. Pastore, and D. M. Perez. Verification of the BISON fuel performance code. *Ann. Nuclear Energy*, 71:81–90, 2014.

[47] D. M. Perez, R. L. Williamson, S. R. Novascone, R. J. Gardner, K. A. Gamble, A. T. Rice, G. Pastore, J. D. Hales, and B. W. Spencer. Assessment of BISON: A nuclear fuel performance analysis code. Technical Report INL/MIS-13-30314, Rev. 2, Idaho National Laboratory, September 2015.